Non-destructive in-situ thermometry of a cold Fermi gas via dephasing impurities

Mark T. Mitchison,[1,*] Thomás Fogarty,[2] Giacomo Guarnieri,[1] Steve Campbell,[3] Thomas Busch,[2] and John Goold[1,†]

[1]*School of Physics, Trinity College Dublin, College Green, Dublin 2, Ireland*
[2]*Quantum Systems Unit, Okinawa Institute of Science and Technology Graduate University, Onna, Okinawa 904-0495, Japan*
[3]*School of Physics, University College Dublin, Belfield Dublin 4, Ireland*

(Dated: April 8, 2020)

The precise measurement of low temperatures is a challenging, important and fundamental task for quantum science. In particular, non-destructive in-situ thermometry is highly desirable for cold atomic systems due to their potential for quantum simulation. Here we demonstrate that the temperature of a non-interacting Fermi gas can be accurately inferred from the non-equilibrium dynamics of impurities immersed within it, using an interferometric protocol and established experimental methods. Adopting tools from the theory of quantum parameter estimation, we show that our proposed scheme achieves optimal precision in the relevant temperature regime for degenerate Fermi gases in current experiments. We also discover an intriguing trade-off between measurement time and thermometric precision that is controlled by the impurity-gas coupling, with weak coupling leading to the greatest sensitivities. This is explained as a consequence of the slow decoherence associated with the onset of the Anderson orthogonality catastrophe, which dominates the gas dynamics following its local interaction with the immersed impurity.

Temperature measurements are crucial for many experiments using ultracold atomic gases, for example when calibrating quantum simulators [1, 2] or when determining equations of state [3, 4]. Unfortunately, standard thermometry techniques such as time-of-flight or in-situ absorption imaging are inherently destructive and require integration over the line of sight [5]. A minimally disturbing method to probe *local* temperature profiles would be beneficial for numerous experimental scenarios of current interest, such as thermalisation dynamics after a quench [6–10] or energy transport between separate thermal reservoirs [11, 12]. Further motivation is provided by recent progress in the preparation of homogeneous ultracold gases [13–19], whose constant density distribution does not carry information on temperature, thus rendering standard in-situ thermometry techniques ineffective.

An appealing alternative method of in-situ thermometry exploits impurity atoms as probes embedded within the ultracold gas [20–23]. The advantage of this approach is that a single atom can be confined to sub-micron length scales and its state is relatively easy to characterise. For example, temperature can be inferred by allowing the impurities to completely equilibrate with the host gas and then measuring their mean energy or a similar observable [24–26]. This method has been successfully used in several recent experiments [27–33] but becomes challenging at low temperatures where equilibration proceeds slowly and the probe's energy levels must be finely tuned [34–39]. These limitations can be overcome by harnessing the probe's *non-equilibrium* dynamics for thermometry [24, 40–44]. Perhaps the most extreme example is pure dephasing, where the energy of the probe is conserved and thus normal thermalisation is completely suppressed. Nevertheless, coherences between the probe energy eigenstates can develop into correlations with the environment that are sensitive to temperature [45–48].

In this letter, we apply this idea to address a long-standing challenge in cold-atom physics: namely, thermometry of degenerate Fermi gases [49, 50]. Specifically, we propose to measure the temperature of an ultracold Fermi gas by observing the non-equilibrium dephasing dynamics of impurities immersed within it. We focus on a promising setup that has already been realised in the laboratory [51, 52], where the gas atoms effectively interact only with the impurities and not with each other. In this setting, the Anderson orthogonality catastrophe (OC) [53, 54] imprints characteristic signatures on the decoherence dynamics of the impurity [55–58], which can be observed using Ramsey interferometry [52, 59, 60]. The optimal precision of our thermometry protocol can be evaluated in terms of the quantum Fisher information, and we reveal a trade-off between measurement time and precision controlled by the impurity-gas interaction strength. Since this coupling can in principle be experimentally tuned over a wide range of values by means of Feshbach resonances [61], our approach allows for precise in-situ thermometry of homogeneous Fermi gases in the deeply degenerate regime.

Thermometry by qubit dephasing.—Let us begin with the general scenario of a two-level probe (qubit) S undergoing pure dephasing due to its contact with an environment E. The total Hamiltonian is $\hat{H} = \hat{H}_S + \hat{H}_E + \hat{H}_I$, where $\hat{H}_I$ is an interaction which satisfies $[\hat{H}_S, \hat{H}_I] = 0$. We assume that the system is initially prepared in the product state $\hat{\rho} = |+\rangle\langle+| \otimes \hat{\rho}_E(T)$, where $\hat{\rho}_E(T)$ is a thermal state of the environment at temperature T and $|+\rangle = (|0\rangle + |1\rangle)/\sqrt{2}$ is an equal superposition of the energy eigenstates of the qubit. The populations of these eigenstates are strictly conserved in time, while the qubit coherences decay according to the decoherence function

$$\nu(t) = \mathrm{Tr}_E\left[e^{i\hat{H}_1 t/\hbar} e^{-i\hat{H}_0 t/\hbar} \hat{\rho}_E(T)\right], \tag{1}$$

where $\hat{H}_j = \langle j|\hat{H}_E + \hat{H}_I|j\rangle$ is the Hamiltonian of the environment conditioned on the qubit eigenstate $j = 0, 1$. In a frame rotating at the qubit precession frequency, the state of the qubit is given by $\hat{\rho}_S = \frac{1}{2}(1 + \mathbf{v}\cdot\hat{\boldsymbol{\sigma}})$, where $\mathbf{v} = (\mathrm{Re}[\nu], \mathrm{Im}[\nu], 0)$ is the Bloch vector and $\hat{\boldsymbol{\sigma}} = (\hat{\sigma}_x, \hat{\sigma}_y, \hat{\sigma}_z)$ are Pauli matrices.

The initial temperature of the gas therefore parametrises the probe state $\hat{\rho}_S(T)$ via the decoherence function in Eq. (1) and

if the dependence of $\nu(t)$ on T is well understood, this temperature can be inferred from the statistics of measurements made on a large ensemble of identically prepared probes. However, any such temperature estimate carries an unavoidable uncertainty due to the random character of quantum measurement and the finite size of the ensemble. We therefore use the theory of quantum parameter estimation to determine the optimal measurement that minimises this uncertainty [62–64].

In general, a measurement is described by a positive operator-valued measure (POVM) $\{\hat{\Pi}(\xi)\}$ satisfying $\int \mathrm{d}\xi\, \hat{\Pi}(\xi) = \mathbb{1}$, where ξ labels the possible outcomes. Performing N independent measurements on identical qubit preparations yields the random outcomes $\boldsymbol{\xi} = \{\xi_1, \xi_2, \ldots, \xi_N\}$, which can be used to generate a temperature prediction via an estimator function $T_{\mathrm{est}}(\boldsymbol{\xi})$. We consider unbiased estimators with $\mathbb{E}[T_{\mathrm{est}}] = T$, where

$$\mathbb{E}\left[T_{\mathrm{est}}\right] = \int \mathrm{d}\xi_1 \cdots \int \mathrm{d}\xi_N\, p(\xi_1|T) \cdots p(\xi_N|T) T_{\mathrm{est}}(\boldsymbol{\xi}), \quad (2)$$

and $p(\xi|T) = \mathrm{Tr}[\hat{\Pi}(\xi)\hat{\rho}_S(T)]$. The expected uncertainty of the temperature estimate is quantified by $\Delta T^2 = \mathbb{E}[(T_{\mathrm{est}} - T)^2]$ and the error of any unbiased estimator obeys the quantum Cramér-Rao bound $\Delta T^2 \geq 1/N\mathcal{F}_T \geq 1/N\mathcal{F}_T^{\mathcal{Q}}$ [65]. Here $\mathcal{F}_T$ is the Fisher information associated with the measurement,

$$\mathcal{F}_T = \int \mathrm{d}\xi\, p(\xi|T) \left(\frac{\partial \ln p(\xi|T)}{\partial T}\right)^2 = \frac{1}{\langle \Delta \hat{X}^2 \rangle} \left(\frac{\partial \langle \hat{X} \rangle}{\partial T}\right)^2, \quad (3)$$

and the second equality holds for projective measurements on a two-level system, with $\langle \hat{X} \rangle$ and $\langle \Delta \hat{X}^2 \rangle$ being the mean and variance of the measured observable $\hat{X}$ as functions of temperature. The Fisher information of any POVM is bounded by the quantum Fisher information (QFI) $\mathcal{F}_T^{\mathcal{Q}} = \max_{\hat{X}} \mathcal{F}_T(\hat{X}) = \mathcal{F}_T(\hat{\Lambda}_T)$ and the maximum is achieved by projective measurements of a specific observable: the symmetric logarithmic derivative (SLD), denoted by $\hat{\Lambda}_T$ [62]. It is convenient to also define the quantum signal-to-noise ratio (QSNR) $\mathcal{Q}^2 = T^2\mathcal{F}_T^{\mathcal{Q}}$, which bounds the signal-to-noise ratio as $T/\Delta T \leq \sqrt{N}\mathcal{Q}$. Hence, $\mathcal{Q}$ quantifies the ultimate sensitivity limit of our impurity thermometer.

For a qubit probe, the QFI has a simple expression in terms of the Bloch vector [66], and for pure dephasing it can be conveniently written in polar coordinates using $\nu = |\nu|e^{i\phi}$ as

$$\mathcal{F}_T^{\mathcal{Q}} = \frac{1}{1 - |\nu|^2} \left(\frac{\partial |\nu|}{\partial T}\right)^2 + |\nu|^2 \left(\frac{\partial \phi}{\partial T}\right)^2 = \mathcal{F}_T^{\parallel} + \mathcal{F}_T^{\perp}. \quad (4)$$

One can see that the QFI comprises two terms, respectively corresponding to the Fisher information for measurements of $\hat{\sigma}_{\parallel} = \cos(\phi)\hat{\sigma}_x + \sin(\phi)\hat{\sigma}_y$ and $\hat{\sigma}_{\perp} = \sin(\phi)\hat{\sigma}_y - \cos(\phi)\hat{\sigma}_x$, i.e. parallel and perpendicular to the Bloch vector of $\hat{\rho}_S(T)$. Up to irrelevant shift and scale factors, the SLD is then given by

$$\hat{\Lambda}_T \propto \cos(\varphi)\hat{\sigma}_{\parallel} + \sin(\varphi)\hat{\sigma}_{\perp}, \quad \tan(\varphi) = \frac{|\nu|(1 - |\nu|)^2 \partial_T \phi}{\partial_T |\nu|}. \quad (5)$$

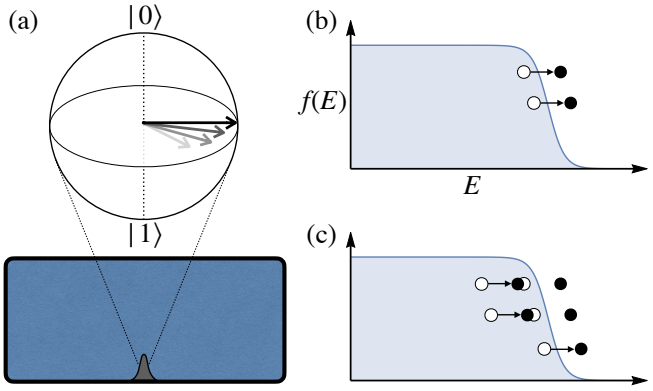

FIG. 1. Schematic depiction of the system. (a) A cold Fermi gas (blue) is perturbed by a localised impurity (grey) with two internal states that undergo pure dephasing. (b) Scattering from the impurity disturbs the atoms' initial equilibrium distribution, $f(E)$. Pauli blocking restricts the resulting particle-hole excitations to a region near the Fermi surface. (c) The creation of holes eventually allows further scattering to generate excitations deep within the Fermi sea.

Since the SLD is optimal in the sense of the quantum Cramér-Rao bound, measuring $\hat{\Lambda}_T$ minimises the uncertainty in the temperature estimate due to the finite number of samples. Note that the SLD is temperature-dependent and thus some prior knowledge of T must be available. In order to measure $\hat{\Lambda}_T$ in practice, one needs an efficient prescription to evaluate $|\nu|$, ϕ and their temperature derivatives from an accurate theoretical model for $\hat{\rho}_S(T)$, as well as the ability to measure an arbitrary combination of $\hat{\sigma}_x$ and $\hat{\sigma}_y$.

Physical model.— We now focus on a physical scenario realised in recent experiments [52], which satisfies all the aforementioned desiderata for optimal thermometry. Here, the qubit comprises two internal spin states of an impurity immersed in a spin-polarised Fermi gas (see Fig. 1). We assume that the impurity is confined to the ground state of a species-selective potential so that its kinetic energy can be neglected. The only relevant collision process at low temperatures is s-wave scattering, which does not occur between identical fermions due to wavefunction anti-symmetry. Therefore, the gas atoms do not interact with each other, while their coupling to the impurity is controlled by a spin-dependent s-wave scattering length. We assume that the impurity and the gas interact only when the impurity is in state $|1\rangle$, which can be achieved by tuning the scattering length for state $|0\rangle$ to zero via a Feshbach resonance [61].

We consider the following interferometric protocol. The gas is prepared in a thermal state with the impurity in the non-interacting state $|0\rangle$, leading to an initial density matrix $\hat{\rho} = |0\rangle\langle 0| \otimes \hat{\rho}_E(T)$. A $\pi/2$-pulse then prepares the superposition state $|0\rangle \to |+\rangle$ and the system freely evolves for a time t, after which the qubit coherences are given by Eq. (1). Finally, a second $\pi/2$-pulse is applied with a phase θ relative to the initial pulse and the qubit's energy is projectively measured, giving a result proportional to $\cos(\theta)\langle\hat{\sigma}_x\rangle + \sin(\theta)\langle\hat{\sigma}_y\rangle$

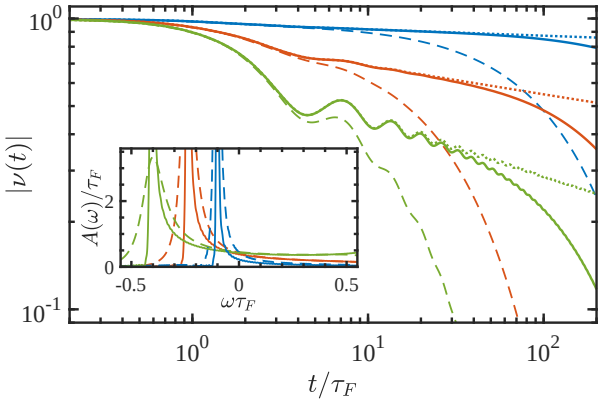

FIG. 2. Decoherence functions (main) and absorption spectra (inset) for the homogeneous gas, with coupling $k_F a = -0.5$ (blue), $k_F a = -1.5$ (red) and $k_F a = -6$ (green); and temperature $T = 0$ (dotted), $T = 0.01T_F$ (solid) and $T = 0.1T_F$ (dashed). Spectra for $T = 0$ not shown.

on average. Repeating this procedure N times — or using N independent impurities interacting with a single copy of the gas — yields the expectation value of any combination of $\hat{\sigma}_x$ and $\hat{\sigma}_y$.

For a non-interacting gas, the decoherence function can be computed *exactly* using the Levitov formula [67, 68]

$$\nu(t) = \det\left[1 - \hat{n} + \hat{n}e^{i\hat{h}_0 t/\hbar}e^{-i\hat{h}_1 t/\hbar}\right], \tag{6}$$

where $\hat{h}_1$ and $\hat{h}_0$ are single-particle Hamiltonians describing the atoms in the gas with or without the presence of the impurity, respectively. The initial thermal distribution is described by $\hat{n} = (e^{\beta(\hat{h}_0-\mu)}+1)^{-1}$, with $\beta = 1/k_B T$ the inverse temperature and μ the chemical potential. In general, we have

$$\hat{h}_0 = \frac{-\hbar^2}{2m}\nabla^2 + V_{\text{ext}}(\mathbf{r}), \tag{7}$$

$$\hat{h}_1 = \hat{h}_0 + V_{\text{imp}}(\mathbf{r}), \tag{8}$$

where m is the atomic mass, $V_{\text{ext}}(\mathbf{r})$ is an external potential, $V_{\text{imp}}(\mathbf{r}) = \int d\mathbf{r}' V_{\text{int}}(\mathbf{r}-\mathbf{r}')|\phi(\mathbf{r}')|^2$ is the scattering potential generated by a static impurity with wavefunction $\phi(\mathbf{r})$, and $V_{\text{int}}(\mathbf{r})$ is the interatomic interaction potential. Collisions in the s-wave channel are described by the regularised pseudopotential $V_{\text{int}}(\mathbf{r}) = \kappa\delta(\mathbf{r})(\partial/\partial r)r$, where $\kappa = 2\pi\hbar^2 a/m_{\text{red}}$ with a the scattering length and m_{red} the reduced mass [69]. Crucially, Eq. (6) replaces a complex many-body expectation value with a determinant over single-particle states, which allows for efficient and accurate computation of a temperature estimate from the experimental data.

Decoherence in a homogeneous gas.—From here on, we focus on a three-dimensional (3D), homogeneous Fermi gas ($V_{\text{ext}} = 0$) of mean density $\bar{n}$ that is trapped in a box large enough to prevent finite-size effects. The impurity is assumed to be tightly confined so that the infinite-mass approximation is valid, i.e. $|\phi(\mathbf{r})|^2 \approx \delta(\mathbf{r})$ and $m_{\text{red}} = m$. Analytical solutions for the single-particle wavefunctions are available in this case [60]; see the Appendix for details. The relevant physical scales of the gas are determined by the Fermi wavevector $k_F = (6\pi^2\bar{n})^{1/3}$, energy $E_F = \hbar^2 k_F^2/2m$, time $\tau_F = \hbar/E_F$ and temperature $T_F = E_F/k_B$, while the impurity-gas coupling is quantified by the dimensionless parameter $k_F a$. The time evolution of the magnitude of the decoherence function for this system is shown in Fig. 2 for various coupling strengths and temperatures. We also plot the corresponding finite-temperature absorption spectra, which are related to $\nu(t)$ by a Fourier transform

$$A(\omega) = \pi^{-1}\text{Re}\int_0^\infty dt\, e^{-i\omega t}\nu(t). \tag{9}$$

Note that $A(\omega)$ is equivalent to the probability distribution of work performed by suddenly switching on the impurity potential $V_{\text{imp}}(\mathbf{r})$ [56, 70]. Since the properties of $\nu(t)$ and $A(\omega)$ have been extensively discussed in the literature [23, 53, 59, 60, 71], here we simply summarise the notable features.

Scattering from the impurity generates particle-hole excitations in the gas. For weak coupling and low temperature, these excitations are initially limited to the vicinity of the Fermi surface due to Pauli blocking (see Fig. 1), but repeated scattering events eventually reorganise the entire Fermi sea: this is the essence of the OC [53]. Fig. 2 shows that at relatively short times, $\tau_F < t \ll \hbar/k_B T$, the OC manifests itself in a universal decoherence behaviour $\nu(t) \sim e^{i\Delta E t/\hbar} t^{-(\delta_F/\pi)^2}$, where $\delta_F = -\arctan(k_F a)$ is the scattering phase at the Fermi surface and ΔE is the energy difference between the many-body ground states of $\hat{H}_0$ and $\hat{H}_1$ [60]. This short-time behaviour is essentially dictated by the high-frequency tails of $A(\omega)$, which describe collective excitations of the whole Fermi sea and thus are largely insensitive to temperature. At later times, the decoherence function departs from the zero-temperature behaviour, decaying exponentially with a temperature-dependent rate for $t \gg \hbar/k_B T$. This long-time behaviour is determined by low-energy excitations close to the Fermi surface whose distribution is highly temperature-dependent. This can be seen in the dominant feature of the absorption spectra near $\omega = \Delta E$ where the zero-temperature edge singularity [71], resulting from the discontinuous Fermi surface, is softened at finite temperature into a broad peak (see Fig. 2 inset). The width of the peak is determined not only by the temperature but also by the scattering length: larger values of $|k_F a|$ lead to a broader peak and thus a faster onset of exponential decay in the time domain.

Thermometric performance.—Let us now turn to the metrological implications of these features. Fig. 3 shows the QSNR as a function of time and temperature for $k_f a = -0.5$. At a given temperature, the optimal measurement time corresponds to the maximum sensitivity, i.e. $\mathcal{Q}_{\max} = \max_t \mathcal{Q}(t) = \mathcal{Q}(t_{\max})$, which can be seen to shift to progressively later times as the temperature decreases. We find that the maximum QSNR, shown by the large yellow region in Fig. 3, coincides with the relevant temperature range for current experiments [72], i.e. $T \gtrsim 0.1T_F$, and good precision is retained down to the deeply degenerate regime. For example, with a coupling

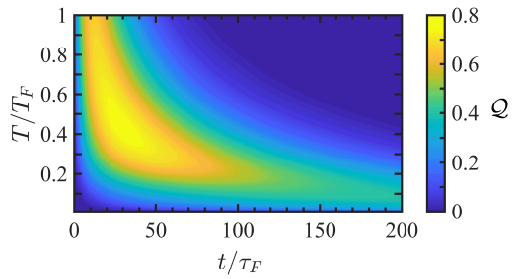

FIG. 3. QSNR as a function of temperature and evolution time for $k_F a = -0.5$.

strength of $k_F a = -0.5$ and a temperature of $T = 0.1T_F$ we find $\mathcal{Q}_{\max} \approx 0.45$, meaning that an error of $\Delta T/T = 10\%$ can be achieved with $N \approx 500$ measurements after a time $t_{\max} \approx 150\tau_F$, which is on the order of milliseconds for typical experimental parameters. This is eminently feasible, since a single gas sample may include thousands of independent impurities [52] and have a lifetime of several seconds [16, 28].

Naturally, the maximum precision is strongly dependent on the coupling strength. In Fig. 4(a) we show the dynamical QSNR for various scattering lengths finding, remarkably, that weaker coupling enhances the thermometric performance. This can be understood by virtue of Eq. (4), which shows that probe states with high purity, i.e. large $|\nu|$, have a larger QFI. Indeed, a state with high purity may have a sharply peaked distribution of measurement outcomes, meaning that a small parameter change is statistically easier to distinguish. Weak coupling is then preferable in light of the slower initial power-law decoherence — due ultimately to Pauli exclusion reducing the available phase space for scattering — which maintains purer, and therefore more sensitive, probe states. This is also illustrated in Fig. 4(b), which shows the path traced by the Bloch vector for two nearby temperatures and two coupling strengths. Clearly, weaker coupling ensures that the probe maintains larger purities and consequently is more sensitive to small changes in temperature. In Fig. 4(c) we show that $\mathcal{Q}_{\max}$ is always larger for smaller scattering strengths, indicating that this qualitative picture holds for all temperatures.

However, this improved precision comes at the cost of measurement time. Indeed, from Fig. 2 we know that the onset of thermal behaviour is delayed by weak coupling. We quantitatively examine the thermometric implications of this in Fig. 4(d) where we find that both $\mathcal{Q}_{\max}$ and $t_{\max}$ diverge as $|k_F a| \to 0$. In this limit, the QFI is dominated by $\mathcal{F}_T^{\perp}$, i.e. the second contribution to Eq. (4), while the SLD is approximately $\hat{\Lambda}_T \approx \hat{\sigma}_{\perp}$. This indicates that it is the phase rather than the amplitude of the probe's coherence that is most sensitive to temperature in this regime. Correspondingly, the optimal measurement becomes equivalent to a *unitary* phase estimation protocol [62, 63]. The universal OC physics is therefore crucial since it provides the slow decoherence which allows for the long times needed for temperature-dependent phase accumulation without sacrificing the purity of the probe state.

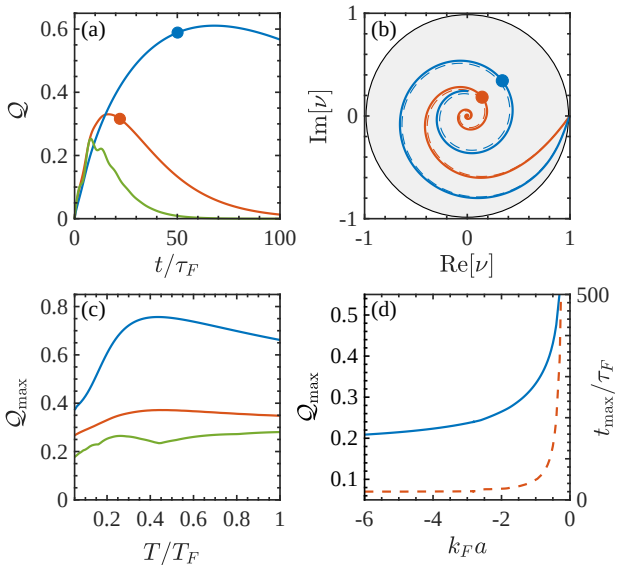

FIG. 4. (a) QSNR at $T = 0.2T_F$ as a function of time for $k_F a = -0.5$ (blue), $k_F a = -1.5$ (red) and $k_F a = -6$ (green). (b) Decoherence function on the equator of the Bloch sphere for $T = 0.2T_F$ (solid lines) and $T = 0.22T_F$ (dashed lines) with $k_F a = -0.5$ (blue) and $k_F a = -1.5$ (red). Solid circles highlight the same instants in time in both panels. (c) Maximum sensitivity, $\mathcal{Q}_{\max}$, as a function of temperature for $k_F a = -0.5$ (blue), $k_F a = -1.5$ (red) and $k_F a = -6$ (green). (d) $\mathcal{Q}_{\max}$ (solid line) and corresponding measurement time (dashed line) as a function of coupling strength for $T = 0.1T_F$. See text for discussion.

Discussion.—Homogeneous ultracold gases represent a challenge for in-situ thermometry, necessitating destructive time-of-flight measurements [13, 16]. In fermionic systems this problem is exacerbated because the Pauli exclusion principle restricts thermal excitations to a small energy window near the Fermi surface, meaning that density measurements of any kind provide little information on temperature. In contrast, our proposal to infer temperature from decoherence is designed to exploit this structure of the Fermi sea. In particular, exclusion effects slow the decay of the impurity decoherence function, allowing for enhanced sensitivity. This is dramatically different from the exponential decoherence that is typically expected, e.g. due to Ohmic noise [48]. Moreover, our scheme is inherently non-equilibrium, thus alleviating the need for thermalisation of the probe before accurate temperature estimation is feasible.

The sensitivity of our probe can be controlled by using a Feshbach resonance to change the scattering length. Remarkably, we have shown that the highest QSNR is obtained for *weak* coupling, in direct contrast with the sensitivity enhancement found for thermalising probes at strong coupling [37]. Practically speaking, weak coupling reduces the number of measurements needed to achieve a given precision, albeit at the cost of increasing the measurement time (and vice versa). This tunability allows the protocol to be optimised depending on the experimental constraints at hand. It is also worth noting that the impurity decoherence function exhibits a universal

dependence on a small number of parameters, $k_F a$, E_F and T, which can each be determined via a similar interferometric protocol. For example, either $k_F a$ or E_F can be determined from the temperature-independent behaviour of $v(t)$ at short times. This may assist calibration of the thermometer and obviates the need to incorporate independent measurements of the density or scattering length — with their associated experimental uncertainties — into the parameter estimation procedure.

Our analysis has focussed on the homogeneous gas where in-situ thermometry via conventional means is difficult. However, the same approach could in principle be applied to trapped gases with arbitrary geometry. In the Appendix, we present results for the one-dimensional (1D) Fermi gas, finding similar thermometric sensitivities to the 3D case. Interestingly, the norm of the decoherence function turns out to be very similar for the homogeneous and the harmonically trapped 1D gas (for $\omega_0 t \ll \pi$, with ω_0 the trap frequency [55]). However, the complex phase of $v(t)$ is significantly modified by the presence of the harmonic trap. Since this phase is generally sensitive to temperature, an optimally precise temperature estimator for a harmonically confined gas should account for the trap configuration. We emphasise that the Levitov formula, Eq. (6), on which our theory is based is computationally efficient for any size and geometry, as it requires only the single-particle wavefunctions.

In summary, we have proposed a minimally destructive and local thermometry protocol based on the decoherence of immersed impurities, which offers a solution to the challenge of in-situ thermometry for cold homogeneous Fermi gases. Future work will address how precision is affected by correlations between impurities generated indirectly via their mutual interaction with the gas [24, 73, 74].

Acknowledgments.— We acknowledge support from the European Research Council Starting Grant ODYSSEY (G. A. 758403), the JSPS KAKENHI-18K13507, the SFI-Royal Society University Research Fellowship scheme, the Science Foundation Ireland Starting Investigator Research Grant "SpeedDemon" (No. 18/SIRG/5508), and the Okinawa Institute of Science and Technology Graduate University.

* mark.mitchison@tcd.ie
† gooldj@tcd.ie

[1] W. Hofstetter and T. Qin, J. Phys. B: At. Mol. Opt. Phys. **51**, 082001 (2018).
[2] L. Tarruell and L. Sanchez-Palencia, C. R. Physique **19**, 365 (2018).
[3] N. Navon, S. Nascimbène, F. Chevy, and C. Salomon, Science **328**, 729 (2010).
[4] M. J. H. Ku, A. T. Sommer, L. W. Cheuk, and M. W. Zwierlein, Science **335**, 563 (2012).
[5] M. Inguscio, W. Ketterle, and C. Salomon, Proc. Int. Sch. Phys. Fermi **164**, 1 (2007).
[6] L. E. Sadler, J. M. Higbie, S. R. Leslie, M. Vengalattore, and D. M. Stamper-Kurn, Nature **443**, 312 (2006).
[7] S. Hofferberth, I. Lesanovsky, B. Fischer, T. Schumm, and J. Schmiedmayer, Nature **449**, 324 (2007).
[8] S. Trotzky, Y.-A. Chen, A. Flesch, I. P. McCulloch, U. Schollwck, J. Eisert, and I. Bloch, Nat. Phys. **8**, 325 (2012).
[9] M. Gring, M. Kuhnert, T. Langen, T. Kitagawa, B. Rauer, M. Schreitl, I. Mazets, D. A. Smith, E. Demler, and J. Schmiedmayer, Science **337**, 1318 (2012).
[10] M. Cheneau, P. Barmettler, D. Poletti, M. Endres, P. Schauß, T. Fukuhara, C. Gross, I. Bloch, C. Kollath, and S. Kuhr, Nature **481**, 484 (2012).
[11] J.-P. Brantut, C. Grenier, J. Meineke, D. Stadler, S. Krinner, C. Kollath, T. Esslinger, and A. Georges, Science **342**, 713 (2013).
[12] S. Krinner, T. Esslinger, and J.-P. Brantut, J. Phys. Cond. Matt. **29**, 343003 (2017).
[13] A. L. Gaunt, T. F. Schmidutz, I. Gotlibovych, R. P. Smith, and Z. Hadzibabic, Phys. Rev. Lett. **110**, 200406 (2013).
[14] T. F. Schmidutz, I. Gotlibovych, A. L. Gaunt, R. P. Smith, N. Navon, and Z. Hadzibabic, Phys. Rev. Lett. **112**, 040403 (2014).
[15] N. Navon, A. L. Gaunt, R. P. Smith, and Z. Hadzibabic, Science **347**, 167 (2015).
[16] B. Mukherjee, Z. Yan, P. B. Patel, Z. Hadzibabic, T. Yefsah, J. Struck, and M. W. Zwierlein, Phys. Rev. Lett. **118**, 123401 (2017).
[17] K. Hueck, N. Luick, L. Sobirey, J. Siegl, T. Lompe, and H. Moritz, Phys. Rev. Lett. **120**, 060402 (2018).
[18] B. Mukherjee, P. B. Patel, Z. Yan, R. J. Fletcher, J. Struck, and M. W. Zwierlein, Phys. Rev. Lett. **122**, 203402 (2019).
[19] Z. Yan, P. B. Patel, B. Mukherjee, R. J. Fletcher, J. Struck, and M. W. Zwierlein, Phys. Rev. Lett. **122**, 093401 (2019).
[20] G. Roati, F. Riboli, G. Modugno, and M. Inguscio, Phys. Rev. Lett. **89**, 150403 (2002).
[21] C. Silber, S. Günther, C. Marzok, B. Deh, P. W. Courteille, and C. Zimmermann, Phys. Rev. Lett. **95**, 170408 (2005).
[22] P. Massignan, M. Zaccanti, and G. M. Bruun, Rep. Prog. Phys. **77**, 034401 (2014).
[23] R. Schmidt, M. Knap, D. A. Ivanov, J.-S. You, M. Cetina, and E. Demler, Rep. Prog. Phys. **81**, 024401 (2018).
[24] D. Hangleiter, M. T. Mitchison, T. H. Johnson, M. Bruderer, M. B. Plenio, and D. Jaksch, Phys. Rev. A **91**, 013611 (2015).
[25] L. A. Correa, M. Perarnau-Llobet, K. V. Hovhannisyan, S. Hernández-Santana, M. Mehboudi, and A. Sanpera, Phys. Rev. A **96**, 062103 (2017).
[26] M. Mehboudi, A. Lampo, C. Charalambous, L. A. Correa, M. A. García-March, and M. Lewenstein, Phys. Rev. Lett. **122**, 030403 (2019).
[27] C. Regal, *Experimental realization of BCS-BEC crossover physics with a Fermi gas of atoms*, Ph.D. thesis, University of Colorado (2005).
[28] F. M. Spiegelhalder, A. Trenkwalder, D. Naik, G. Hendl, F. Schreck, and R. Grimm, Phys. Rev. Lett. **103**, 223203 (2009).
[29] S. Nascimbène, N. Navon, K. J. Jiang, F. Chevy, and C. Salomon, Nature **463**, 1057 (2010).
[30] D. McKay and B. DeMarco, New J. Phys. **12**, 055013 (2010).
[31] R. Olf, F. Fang, G. E. Marti, A. MacRae, and D. M. Stamper-Kurn, Nat. Phys. **11**, 720 (2015).
[32] M. Hohmann, F. Kindermann, T. Lausch, D. Mayer, F. Schmidt, and A. Widera, Phys. Rev. A **93**, 043607 (2016).
[33] R. S. Lous, I. Fritsche, M. Jag, B. Huang, and R. Grimm, Phys. Rev. A **95**, 053627 (2017).
[34] L. A. Correa, M. Mehboudi, G. Adesso, and A. Sanpera, Phys. Rev. Lett. **114**, 220405 (2015).

[35] M. G. A. Paris, J. Phys. A: Math. Theor. **49**, 03LT02 (2015).
[36] A. D. Pasquale, D. Rossini, R. Fazio, and V. Giovannetti, Nat. Commun. **7**, 12782 (2016).
[37] K. V. Hovhannisyan and L. A. Correa, Phys. Rev. B **98**, 045101 (2018).
[38] S. Campbell, M. G. Genoni, and S. Deffner, Quantum Sci. Technol. **3**, 025002 (2018).
[39] P. P. Potts, J. B. Brask, and N. Brunner, Quantum **3**, 161 (2019).
[40] S. Jevtic, D. Newman, T. Rudolph, and T. M. Stace, Phys. Rev. A **91**, 012331 (2015).
[41] L. Mancino, M. Sbroscia, I. Gianani, E. Roccia, and M. Barbieri, Phys. Rev. Lett. **118**, 130502 (2017).
[42] P. P. Hofer, J. B. Brask, M. Perarnau-Llobet, and N. Brunner, Phys. Rev. Lett. **119**, 090603 (2017).
[43] V. Cavina, L. Mancino, A. De Pasquale, I. Gianani, M. Sbroscia, R. I. Booth, E. Roccia, R. Raimondi, V. Giovannetti, and M. Barbieri, Phys. Rev. A **98**, 050101 (2018).
[44] Q. Bouton, J. Nettersheim, D. Adam, F. Schmidt, D. Mayer, T. Lausch, E. Tiemann, and A. Widera, Phys. Rev. X **10**, 011018 (2020).
[45] M. Bruderer and D. Jaksch, New J. Phys. **8**, 87 (2006).
[46] C. Sabín, A. White, L. Hackermuller, and I. Fuentes, Sci. Rep. **4**, 6436 (2014).
[47] T. H. Johnson, F. Cosco, M. T. Mitchison, D. Jaksch, and S. R. Clark, Phys. Rev. A **93**, 053619 (2016).
[48] S. Razavian, C. Benedetti, M. Bina, Y. Akbari-Kourbolagh, and M. G. A. Paris, Eur. Phys. J. Plus **134**, 284 (2019).
[49] D. C. McKay and B. DeMarco, Rep. Prog. Phys. **74**, 054401 (2011).
[50] R. Onofrio, Physics-Uspekhi **59**, 1129 (2016).
[51] M. Cetina, M. Jag, R. S. Lous, J. T. M. Walraven, R. Grimm, R. S. Christensen, and G. M. Bruun, Phys. Rev. Lett. **115**, 135302 (2015).
[52] M. Cetina, M. Jag, R. S. Lous, I. Fritsche, J. T. M. Walraven, R. Grimm, J. Levinsen, M. M. Parish, R. Schmidt, M. Knap, and E. Demler, Science **354**, 96 (2016).
[53] P. W. Anderson, Phys. Rev. Lett. **18**, 1049 (1967).
[54] T. Fogarty, S. Deffner, T. Busch, and S. Campbell, Phys. Rev. Lett. **124**, 110601 (2020).
[55] A. Sindona, J. Goold, N. Lo Gullo, S. Lorenzo, and F. Plastina, Phys. Rev. Lett. **111**, 165303 (2013).
[56] A. Sindona, J. Goold, N. L. Gullo, and F. Plastina, New J. Phys. **16**, 045013 (2014).
[57] F. Cosco, M. Borrelli, E.-M. Laine, S. Pascazio, A. Scardicchio, and S. Maniscalco, New J. Phys. **20**, 073041 (2018).
[58] F. Tonielli, R. Fazio, S. Diehl, and J. Marino, Phys. Rev. Lett. **122**, 040604 (2019).
[59] J. Goold, T. Fogarty, N. Lo Gullo, M. Paternostro, and T. Busch, Phys. Rev. A **84**, 063632 (2011).
[60] M. Knap, A. Shashi, Y. Nishida, A. Imambekov, D. A. Abanin, and E. Demler, Phys. Rev. X **2**, 041020 (2012).
[61] C. Chin, R. Grimm, P. Julienne, and E. Tiesinga, Rev. Mod. Phys. **82**, 1225 (2010).
[62] M. G. A. Paris, Int. J. Quantum Inf. **07**, 125 (2009).
[63] G. Tóth and I. Apellaniz, J. Phys. A: Math. Theor. **47**, 424006 (2014).
[64] M. Mehboudi, A. Sanpera, and L. A. Correa, J. Phys. A: Math. Theor. **52**, 303001 (2019).
[65] S. L. Braunstein and C. M. Caves, Phys. Rev. Lett. **72**, 3439 (1994).
[66] W. Zhong, Z. Sun, J. Ma, X. Wang, and F. Nori, Phys. Rev. A **87**, 022337 (2013).
[67] D. A. Abanin and L. S. Levitov, Phys. Rev. Lett. **94**, 186803 (2005).
[68] N. d'Ambrumenil and B. Muzykantskii, Phys. Rev. B **71**, 045326 (2005).
[69] T. Busch, B.-G. Englert, K. Rzażewski, and M. Wilkens, Found. Phys. **28**, 549 (1998).
[70] T. Keller and T. Fogarty, Phys. Rev. A **94**, 063620 (2016).
[71] P. Noziéres and C. T. De Dominicis, Phys. Rev. **178**, 1097 (1969).
[72] S. Nascimbène, N. Navon, K. J. Jiang, L. Tarruell, M. Teichmann, J. McKeever, F. Chevy, and C. Salomon, Phys. Rev. Lett. **103**, 170402 (2009).
[73] M. T. Mitchison, T. H. Johnson, and D. Jaksch, Phys. Rev. A **94**, 063618 (2016).
[74] G. Planella, M. Mehboudi, and A. Acin, arXiv:2001.11812 [quant-ph] (2020).
[75] M. Olshanii, Phys. Rev. Lett. **81**, 938 (1998).

Appendix

Calculation of the decoherence function

In this Appendix, we give details on our calculation of the decoherence functions displayed in the main text. We work in spherical coordinates with the impurity placed at $r = 0$ and impose hard-wall boundary conditions at a radius $r = R$. Assuming low temperatures and s-wave scattering, only atoms with zero angular momentum are perturbed by the impurity. Higher partial-wave states thus do not contribute to the determinant in Eq. (6).

The s-wave eigenfunctions of the perturbed and unperturbed Hamiltonians are denoted by $\psi_n(r)$ and $\psi'_n(r)$ respectively, such that $\hat{h}_0\psi_n = E_n\psi_n$ and $\hat{h}_1\psi'_n = E'_n\psi'_n$. They are given explicitly by [60]

$$\psi_n(r) = \sqrt{\frac{1}{2\pi R}}\frac{\sin(k_n r)}{r}, \tag{10}$$

$$\psi'_n(r) = A_n\sqrt{\frac{1}{2\pi R}}\frac{\sin(k'_n r + \delta_n)}{r}, \tag{11}$$

where $k_n R = k'_n R + \delta_n = n\pi$ for $n = 1, 2, \ldots$, while $E_n = \hbar^2 k_n^2/2m$ and $E'_n = \hbar^2 k_n'^2/2m$. The scattering phase is determined by the equation

$$\tan(\delta_n) = -k'_n a, \tag{12}$$

while $A_n = \left[1 + \sin(2\delta_n)/2k'_n R\right]^{-1/2}$. Here we have assumed negative scattering lengths so that no bound state arises.

The Fermi energy is determined by $E_F = \hbar^2 k_F^2/2m = \pi^2\hbar^2 N_s^2/2mR^2$, where N_s is the number of atoms in s states at $T = 0$. We work at fixed 3D density and thus hold E_F fixed, which is equivalent to fixing the ratio $N_s/R = \sqrt{2mE_F}/\pi\hbar$. All of our results are scaled to the thermodynamic limit by increasing N_s until convergence is achieved. On the timescales we consider, N_s on the order of a few hundred is sufficient.

The determinant in Eq. (6) is infinite-dimensional in principle, but at any given density and temperature it can be computed to high accuracy within a finite basis set. The size N of the unperturbed basis set $\{\psi_n\}_{n=1}^N$ is fixed by the temperature

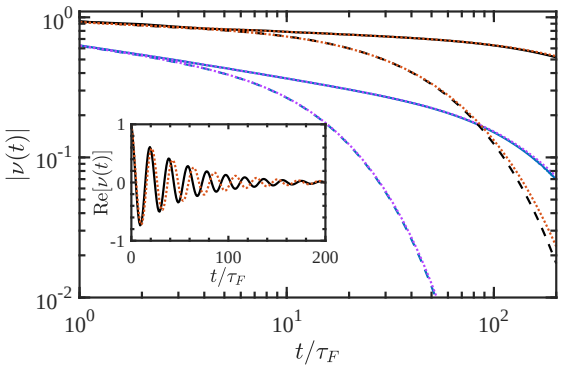

FIG. 5. Comparison of decoherence functions for a homogeneous and a harmonically trapped gas in 1D. The main panel shows the absolute value for the homogeneous gas at couplings $k_F a = -1$ (black) and $k_F a = -0.01$ (blue) with temperatures $T = 0.01 T_F$ (solid) and $T = 0.1 T_F$ (dashed). Red and purple dotted lines show the corresponding results for a harmonically confined gas with $\hbar\omega_0/E_F = 2.5 \times 10^{-3}$. The inset displays the real part of the decoherence function for $k_F a = -1$ and $T = 0.1 T_F$.

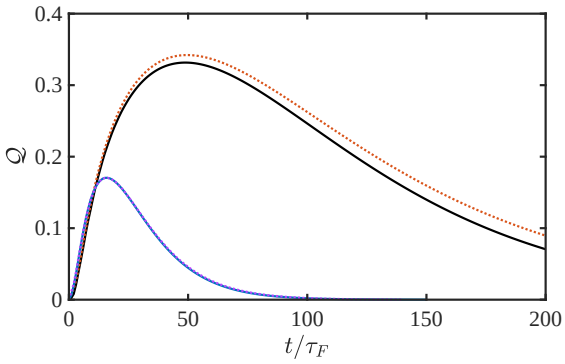

FIG. 6. Comparison of the QSNR for a homogeneous (solid) and a harmonically trapped (dotted) gas in 1D at temperature $T = 0.1$ and coupling strengths $k_F a = -1$ (black, red) and $k_F a = -0.01$ (blue, purple).

and N_s. For each value of T, we find the chemical potential by solving $\mathrm{Tr}[\hat{n}] = N_s$ with a very large basis ($\sim 10^4$ states). We then truncate to N states such that $|\mathrm{Tr}[\hat{n}] - N_s| < \epsilon$, where ϵ is a small tolerance. The size of the perturbed basis set $\{\psi'_n\}_{n=1}^{N'}$ is then fixed by the requirement of unitarity: $\sum_{n=1}^{N'} |\langle\psi_m|\psi'_n\rangle|^2 > 1 - \epsilon$ for all $m \leq N$. We find that $\epsilon = 10^{-4}$ is sufficient to obtain good convergence.

The Fisher information is evaluated via a finite-difference approximation to the temperature derivatives in Eq. (4) with numerical increments of $\delta T/T = 10^{-2}$.

One-dimensional and harmonically trapped systems

In this Appendix, we discuss how reduced spatial dimensionality and the presence of a harmonic trap affect the sensitivity of our dephasing thermometer. To be concrete, we focus on a one-dimensional (1D) system. In this case, the impurity-gas interaction is described in the pseudo-potential approximation by $V_{\mathrm{imp}}(x) = \lambda\delta(x)$, with $\lambda = -\hbar^2/m_{\mathrm{red}}a$ [75]. Note that the interaction strength is inversely proportional to the scattering length in 1D. We consider a tightly localised impurity at $x = 0$ so that $m_{\mathrm{red}} = m$ and $|\phi(x)|^2 \approx \delta(x)$.

Let us first consider a homogeneous gas and impose hard-wall boundary conditions at $x = \pm L/2$. Only the wavefunctions with even symmetry are perturbed by the presence of the impurity at $x = 0$; the odd solutions thus do not contribute to the determinant in Eq. (6). The even eigenfunctions of $\hat{h}_0$ and $\hat{h}_1$ are respectively found to be

$$\psi_n(x) = \sqrt{\frac{2}{L}}\cos(k_n x), \tag{13}$$

$$\psi'_n(x) = B_n\sqrt{\frac{2}{L}}\cos(k'_n x \pm \delta_n), \tag{14}$$

where the plus (minus) sign pertains to $x > 0$ ($x < 0$) and $k_n L = k'_n L + 2\delta_n = (2n-1)\pi$ for $n = 1, 2, \ldots$, while the corresponding energies are $E_n = \hbar^2 k_n^2/2m$ and $E'_n = \hbar^2 k'^2_n/2m$. Note that here we assume negative scattering length; for $a > 0$ the $n = 1$ solution is a bound state that must be accounted for separately. The scattering phase is determined by the equation

$$\tan(\delta_n) = \frac{1}{k'_n a}, \tag{15}$$

while $B_n = [1 - \sin(2\delta_n)/k'_n L]^{-1/2}$. Similar to the 3D case, holding the density fixed leads to the relation $(2N_e - 1)/L = \sqrt{2mE_F}/\pi\hbar$, where N_e is the number of atoms in even states. We follow the same procedure as in the 3D case to find the truncated bases for a given value of N_e, and then scale to the thermodynamic limit by increasing N_e until convergence is reached.

Some examples of the decoherence function are plotted in Fig. 5 for different coupling strengths and temperatures. The qualitative behaviour is similar to the 3D case. The short-time behaviour of $\nu(t)$ is an oscillatory power-law decay that passes over to exponential decay after a time on the order of $\hbar/k_B T$. In Fig. 6 we show the QSNR, finding similar results to the 3D case. In particular, we find again that weaker coupling, corresponding in 1D to larger scattering length, yields higher precision. However, we leave a careful exploration of the thermometric sensitivity in 1D to future work.

In order to understand the role of weak harmonic confinement, we also consider the case where the 1D gas is trapped by the harmonic potential $V_{\mathrm{ext}}(x) = \frac{1}{2}m\omega_0^2 x^2$. While

in this case analytical solutions for the perturbed eigenfunctions are known [69], we resort to numerical diagonalisation of $\hat{h}_0$ and $\hat{h}_1$ for simplicity. Again, reflection symmetry implies that only the even wavefunctions enter non-trivially into the determinant. The corresponding unperturbed energies are $E_n = \hbar\omega_0\left(2n + \frac{1}{2}\right)$ for $n = 0, 1, \ldots$. If N_e atoms occupy even orbitals at $T = 0$, the Fermi energy is thus defined by $E_F = \hbar\omega_0\left(2N_e - \frac{3}{2}\right)$, from which the Fermi wavevector $k_F = \sqrt{2mE_F}/\hbar$, temperature $T_F = E_F/k_B$ and time $\tau_F = \hbar/E_F$ can be derived. We hold E_F constant, which is equivalent to keeping the density at the centre of the trap fixed. We also assume weak confinement, $\hbar\omega_0 \ll E_F$, and focus on times less than the trap half-period, $\omega_0 t < \pi$, in order to avoid partial recurrences [55, 56]. Our numerical calculations follow the same truncation procedure described above.

The decoherence function for the harmonically trapped gas is compared to the homogeneous case in Fig. 5. We find that the norm of the decoherence function is very similar in both cases (main panel) but the phase of the decoherence function is noticeably different (inset). As a consequence, a temperature estimator based on the norm of the decoherence function may not need to account for details of the trap potential in the weakly confined regime. However, as discussed in the main text, at weak coupling the SLD becomes very sensitive to the phase of $v(t)$. The trap geometry must therefore be taken explicitly into account in order to achieve the highest precision. As shown in Fig. 6, the optimal precision attainable in the trapped gas is very similar to that of the homogeneous gas.